ChemPubSoc Europe

DOI: 10.1002/chem.201702687

CHEMISTRY
A European Journal
Communication

Nanoparticles | *Very Important Paper*

VIP Prussian Blue-Derived Synthesis of Hollow Porous Iron Pyrite Nanoparticles as Platinum-Free Counter Electrodes for Highly Efficient Dye-Sensitized Solar Cells

Jeffrey E. Chen,[a, b] Miao-Syuan Fan,[a] Yen-Lin Chen,[a] Yu-Heng Deng,[a] Jung Ho Kim,[c, d] Hatem R. Alamri,[e] Zeid A. Alothman,[f] Yusuke Yamauchi,[c, d, f] Kuo-Chuan Ho,*[a] and Kevin C.-W. Wu*[a]

Abstract: Iron pyrite has long been an attractive material for environmental and energy applications, but is hampered by a lack of control over morphology and purity. Hollow porous iron pyrite nanoparticles were synthesized by a direct sulfurization of iron oxide derived from Prussian blue. The high efficiencies of these hollow porous iron pyrite nanoparticles as effective dye-sensitized solar cell counter electrodes were demonstrated, with an efficiency of 7.31%.

Owing to its high optical absorbance, non-toxicity, global abundance, and suitable band gap, iron pyrite has drawn growing research interests in recent years. Not only has iron pyrite been widely applied in environmental applications for heavy metal absorption,[1–3] iron pyrite has also been identified as a promising material for various energy applications such as lithium-ion battery cathodes,[4] photovoltaic,[5–9] and counter electrodes for dye-sensitized solar cells.[10,11] Considering that size, morphology, and purity of iron pyrite have been attributed as important characteristics for these applications,[12–14] the synthesis of nanostructured pure iron pyrite is of upmost importance.

Iron pyrite synthesis could mainly be categorized into groups of wet-chemical based and sulfurization based.[15] Wet-chemical routes including hydrothermal,[16] solvothermal,[17] hot-injection,[18] and heat-up synthesis[19] have been widely developed for iron pyrite. However, the controllable morphology of high purity iron pyrite still remains a challenge due to the abundance of other iron sulfide stoichiometries (e.g., pyrrhotite, $Fe_{1-x}S$ with $x=0$ to 0.2) and crystallographic forms (e.g., marcasite, orthorhombic FeS_2). On the other hand, sulfurization based routes typically rely on the reaction of either elemental sulfur or H_2S[20] at elevated temperatures with iron precursors, including elemental iron, FeF_3,[4] $FeBr_2$,[7] $Fe(OH)_3$,[12] Fe_2O_3,[21] and Fe_3O_4.[21] Generally, sulfurization is an attractive synthesis route as the size and morphology of iron pyrite could be controlled through that of the iron precursors. Additionally, capping agents and surfactants that are typically present in wet-chemical routes are absent for iron pyrite synthesized through sulfurization.

Among the sulfurization synthesis routes presented in literature, the sulfurization of iron oxides with elemental sulfur has been regarded as one of the most promising sulfurization routes for two main reasons. First, pyrite formation with elemental sulfur is faster than that with H_2S and could generally be achieved at lower temperatures to avoid pyrite decomposition.[20] Second, sulfurization of iron oxides with elemental sulfur has been known to skip the intermediate steps of FeS and FeS_{2-x},[22] resulting in the formation of pure and stoichiometric iron pyrite. However, sulfurization reactions typically suffer from low scalability, with only either iron pyrite thin

[a] J. E. Chen, M.-S. Fan, Y.-L. Chen, Y.-H. Deng, Prof. K.-C. Ho, Prof. K. C.-W. Wu
Department of Chemical Engineering
National Taiwan University
No. 1, Sec. 4, Roosevelt Rd.
Taipei 10617 (Taiwan)
E-mail: kevinwu@ntu.edu.tw
kcho@ntu.edu.tw

[b] J. E. Chen
Department of NanoEngineering
University of California
San Diego, La Jolla, CA 92093 (USA)

[c] Prof. J. H. Kim, Prof. Y. Yamauchi
Australian Institute for Innovative Materials (AIIM)
University of Wollongong
Squires Way
North Wollongong, NSW 2500 (Australia)

[d] Prof. J. H. Kim, Prof. Y. Yamauchi
International Research Center for Materials Nanoarchitectonics (MANA)
National Institute for Materials Science (NIMS)
1-1 Namiki, Tsukuba
Ibaraki 305-0044 (Japan)

[e] Prof. H. R. Alamri
Physics Department
Jamoum University College
Umm Al-Qura University
Makkah 21955 (Saudi Arabia)

[f] Prof. Z. A. Alothman, Prof. Y. Yamauchi
Advanced Materials Research Chair
Chemistry Department, College of Science
King Saud University
Riyadh 11451 (Saudi Arabia)

Supporting information and the ORCID identification number(s) for the author(s) of this article can be found under https://doi.org/10.1002/chem.201702687.

© 2017 Wiley-VCH Verlag GmbH & Co. KGaA, Weinheim

films or nanowires/nanotubes grown on fluorine-doped tin oxide (FTO) substrates. The reason for this limitation could be attributed to the difficulty for gaseous sulfur to penetrate into iron oxide due to oxygen accumulation.[22] Additionally, although the syntheses of hollow nanowires/nanotubes have been demonstrated with the sulfurization of nanowire/nanotube precursors before, no one has yet been able to synthesize hollow iron pyrite nanoparticles.

Recently, coordination polymers including metal-organic frameworks (MOFs), are widely used as supporters for the post-modification of desired structures due to their high chemical stability and rich diversity of metal sources.[23,24] We herein propose the large-scale and high purity synthesis of hollow porous iron pyrite nanoparticles from the sulfurization of Prussian blue (PB) derived iron oxides with elemental sulfur. By using PB, a coordination polymer with a cyano-bridged structure, we propose not only control over morphology, but also the introduction of nanoporous iron oxide structures for highly efficient sulfurization. To demonstrate the advantage of our nanostructured iron pyrite, we have hereby applied our synthesized particles as counter-electrodes (CEs) for dye-sensitized solar cells (DSSCs); an attractive candidate for photovoltaic energy conversion.

Scanning electron microscopy (SEM, Figure 1 a) of the as-synthesized iron pyrite reveals nanoparticles of 150 ± 25 nm with porous features. The transmission electron microscopy (TEM) image in Figure 1 b further confirms the presence of pores and reveals its hollow structure. The hollow porous iron pyrite nanoparticles were hereon referred to as h-FeS_2. Composition and structural analysis of h-FeS_2 were carried out with X-ray diffraction (XRD) and X-ray photoelectron spectrum (XPS). XRD patterns (Figure 1 c–e) reveal the successful sulfurization, with diffraction peaks attributed to iron pyrite (JCPDS #65–3321). No peaks of common iron pyrite contaminants were observed, including those of both pyrrhotite ($Fe_{1-x}S$, $x = 0$ to 0.2; JCPDS #06–0696; Figure 1g) and marcasite (orthorhombic FeS_2, JCPDS #65–2567; Figure 1f). Additionally, no peaks of the original precursor (hematite; JCPDS #86–0550) were observed as well, which indicates that sulfurization was completely carried out. The chemical compositions of the as-synthesized particles were further examined with XPS. Two photoelectron peaks in the Fe 2p region with binding energies at 719.8 and 706.9 eV (Figure 1 h) could be attributed to Fe $2p_{1/2}$ and Fe $2p_{3/2}$ of iron pyrite, respectively. No binding energies corresponding to hematite at 710.3 and 724.1 eV were observed in the Fe 2p region, which further confirms the previous XRD result of complete sulfurization. For the S 2p region (Figure 1 i), photoelectron peaks with binding energies of 163.7 and 162.6 eV correspond to S $2p_{1/2}$ and S $2p_{3/2}$, respectively, which are sulfur binding energies typically found in FeS_2. Photoelectron signals at 161.4 eV were not observed, which indicates the absence of FeS contaminants and the purity of our sulfurized particles.

The schematic diagram in Figure 2 describes the synthesis of the hollow porous iron pyrite nanoparticles. First, PB nanoparticles were synthesized according to our previous reports.[25] The nanoparticles were then chemically etched with HCl solution in the presence of polyvinylpyrrolidone (PVP) as a protective surfactant. This results in the removal of the particle interior and the formation of the hollow structure. Prussian blue was converted to iron oxide by calcination to remove the organic contents (CN bridges), and to oxidize the Fe atoms.[26] The conversion of iron oxide nanoparticles to iron pyrite was completed by sulfurization [Eq. (1)]:

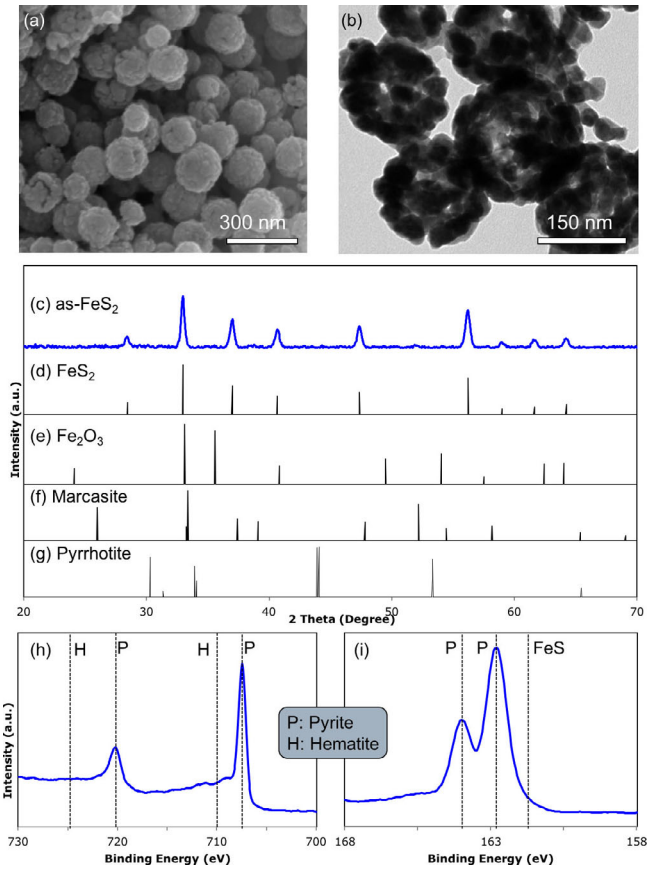

Figure 1. a) SEM and b) TEM images of h-FeS_2. XRD patterns of c) as-synthesized h-FeS_2, d) reference iron pyrite, e) reference α-Fe_2O_3, f) reference marcasite, and g) reference pyrrhotite. XPS spectra of as-synthesized hollow iron pyrite in the h) Fe 2p region and i) S 2p region.

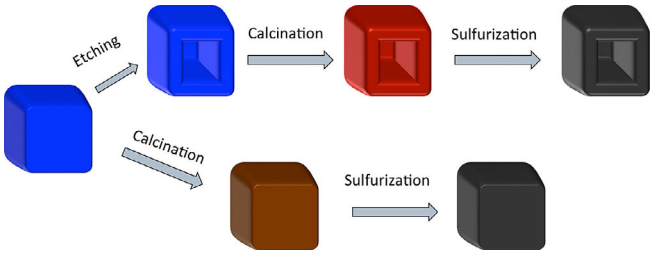

Figure 2. Schematic diagram for the synthesis of hollow iron pyrite (h-FeS_2) nanoparticles and solid iron pyrite (s-FeS_2) nanoparticles.

$$2\,Fe_2O_{3(g)} + 11\,S \rightarrow 4\,FeS_{2(s)} + 3\,SO_{2(g)} \quad (1)$$

The typical sulfurization reaction is carried out at 450 °C for 30 min with a sulfur source of 180 mg for 30 mg iron oxide precursor. Not only is this among one of the shorter sulfuriza-

© 2017 Wiley-VCH Verlag GmbH & Co. KGaA, Weinheim

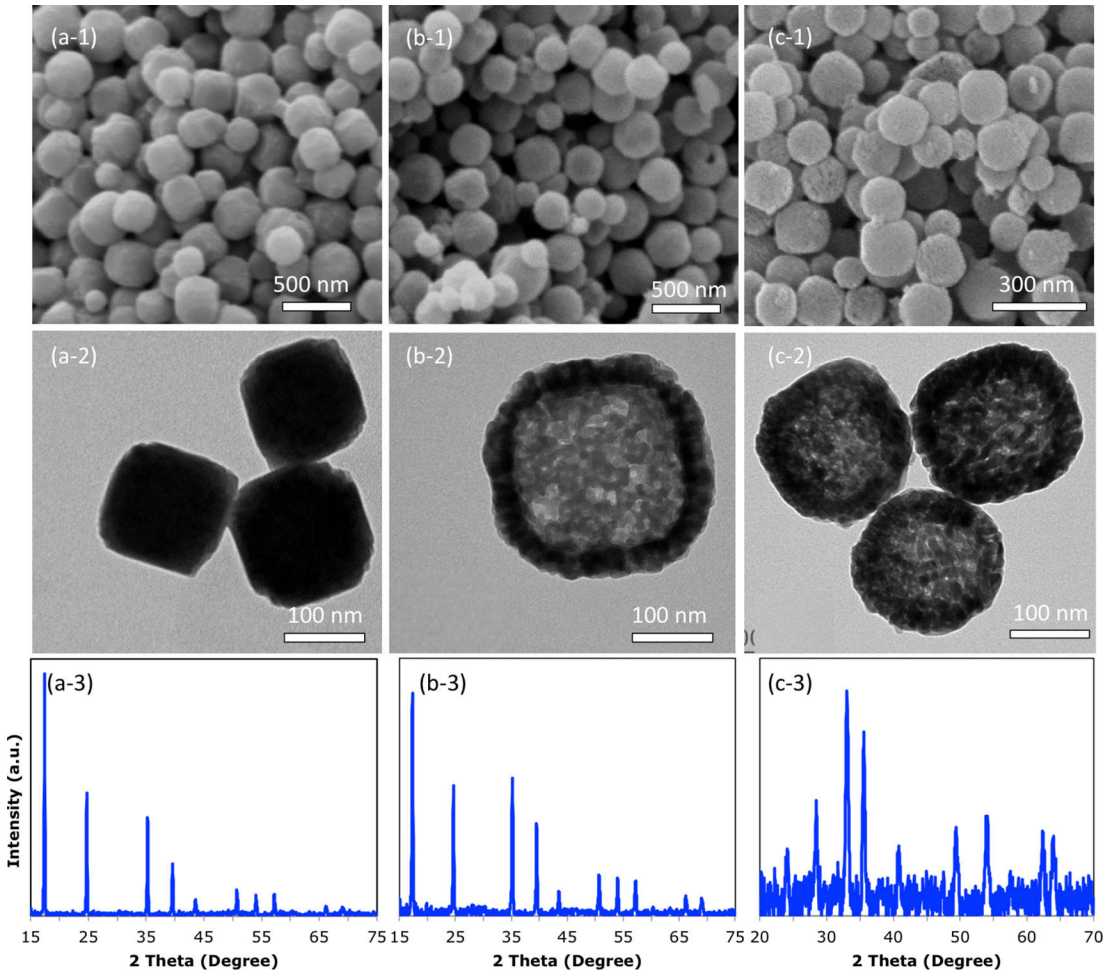

Figure 3. SEM, TEM, and XRD of a) PB, b) hollow PB, and c) iron oxide calcined from hollow PB.

tion durations reported in literature, the amount elemental sulfur powder required is also one of the lowest, especially for an open gas flow reaction. Additionally, 30 mg is among the highest quantity to be sulfurized with an iron oxide precursor and one of the few high-quantity sulfurization reactions. Although the sulfurization of increased amounts of precursors have not been investigated in this study, we believe that our reaction is easily scalable, considering the highly efficient sulfurization reaction.

Precursors for h-FeS_2 were characterized with SEM, TEM, and XRD (Figure 3). As shown in Figure 3a-1, PB particles of $\approx$150 nm were successfully synthesized. TEM (Figure 3a-2) further reveals the solid interior in the particles. After etching (Figure 3b-1), the morphology of the PB nanoparticles remained nearly identical, but with hollow interiors confirmed with TEM (Figure 3b-2). XRD patterns of Prussian blue prior to (Figure 3a-3) and after etching (Figure 3b-3) both reveal the same diffraction peaks, which are in agreement with PB diffraction peaks found in literature (JCPDS #73–0687). After calcination, the morphologies of the particles are still well preserved and indicate minimal structural collapse (Figure 3c). Additional TEM images (Figure 3c-2) further reveal increased pore formation due to the removal of organics. X-ray diffraction patterns (Figure 3c-3) reveal the successful calcination of PB to α-Fe_2O_3 (hematite). All the diffraction peaks at $2\theta = 23.9$, 33.2, 35.2, 40.7, 49.2, 53.9, 62.3, and 63.7 degree are well matched with hematite.

To highlight the hollow and porous nanostructure of h-FeS_2, solid iron pyrite nanoparticles were also synthesized according to the schematic shown in Figure 2. Skipping the etching of PB is the only experimental difference between the two iron pyrite nanoparticles, with the exact calcination and sulfurization conditions maintained. As shown with SEM (Figure S1a-1 in Supporting Information), the particle morphology of iron oxide derived from unetched PB is very similar to that from etched PB. TEM (Figure S1b-1) further suggests pore formation due to the removal of organics, and confirms its non-hollow structure. However, XRD patterns (Figure S2) reveal that instead of the hematite phase that was observed with the hollow PB, the iron oxide was actually amorphous due to hindered air diffusion during calcination.[26] After sulfurization, the particle morphology (Figure S1) became much less defined as compared to its iron oxide precursor. XRD (Figure S2b) and XPS (Figure S2c and d) of the s-FeS_2 confirm iron pyrite of high purity.

© 2017 Wiley-VCH Verlag GmbH & Co. KGaA, Weinheim

The as-synthesized iron pyrite nanoparticles were dispersed in isopropanol and drop-casted onto an FTO substrate without further treatment. The photocurrent density–voltage (*J–V*) curves of the DSSC with the h-FeS_2, s-FeS_2, and platinum (Pt) CEs are shown in Figure 4, and the corresponding photovoltaic parameters are summarized in Table 1. The DSSC employing s-

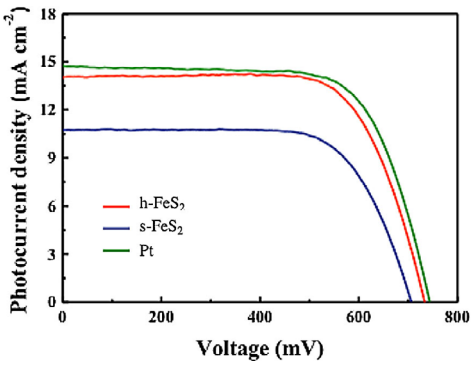

Figure 4. Photocurrent density–voltage (*J–V*) curves of the iron pyrite nanoparticle samples with reference platinum counter electrodes.

Table 1. Photovoltaic parameters of DSSCs using h-FeS_2, s-FeS_2 and Pt CEs.

Sample	η [%]	V_{oc} [mV]	J_{sc} [mA cm^{-2}]	FF
h-FeS_2	7.31	731.66	14.01	0.71
s-FeS_2	5.30	704.80	10.75	0.70
Pt	7.69	740.51	14.66	0.71

FeS_2 CE yielded a photoelectric conversion efficiency (η) of 5.30% with a short-circuit current density (J_{sc}) of 10.75 mA cm^{-2}, open-circuit voltage (V_{oc}) of 704.80 mV, and fill factor (FF) of 0.70. The DSSC with the h-FeS_2 CE showed a higher V_{oc} of 731.66 mV, J_{sc} of 14.01 mA cm^{-2}, and η of 7.31%. In comparison to the h-FeS_2 CE, the DSSC employing the Pt CE produced an η of 7.69% (V_{oc} = 740.51 mV, J_{sc} = 14.66 mA cm^{-2}, and FF = 0.71). The η of the DSSC employing h-FeS_2 CE reached a value of 7.31%, close to that of DSSC using a Pt CE (7.69%). Since FF is about the same in Table 1, the η of the DSSCs depends strongly on the values of V_{oc} and J_{sc}. In fact, the CE served to inject the charge into the electrolyte, thus facilitating the reduction of tri-iodide (I_3^-). The higher V_{oc} for DSSC with an h-FeS_2 CE, as photoanode and electrolyte are the same, illustrates that the h-FeS_2 CE may accelerate the reduction of I_3^- in comparison with s-FeS_2 CE.[27–29] In addition, the higher J_{sc} implies the higher catalytic activity for facilitating the reduction of I_3^-.[30,31] In contrast to the s-FeS_2, the h-FeS_2 CE with hollow structure provided more catalytic surface area, which implied higher catalytic ability, thus enhancing the J_{sc} of DSSC to 14.01 mA cm^{-2}. Overall, the h-FeS_2 demonstrated the potential as a cost-effective and efficient CE material to replace expensive Pt CE in DSSCs.

In summary, here we demonstrate the first synthesis of hollow porous iron pyrite nanoparticles by the sulfurization of iron oxide derived from PB. A highly efficient synthesis with short reaction time of 30 min and low sulfur precursor was achieved. The as-synthesized h-FeS_2 nanoparticles were simply drop casted onto FTO without any further treatment to serve as efficient counter electrodes for DSSCs, with an efficiency of 7.31%

Acknowledgements

The authors would like to thank the Ministry of Science and Technology (MOST), Taiwan (103-2923-E-002-008-MY3, 104-2628-E-002-008-MY3, 105–2221-E-002-229-MY3, and 105-2218-E-155-007) and the National Taiwan University (105R7706) for the funding support. Y.Y. and Z.A.A. are grateful to the Deanship of Scientific Research, King Saud University for funding through Vice Deanship of Scientific Research Chairs. The authors would like to thank Dr. Macs, Bio-Pharma Private Limited, for helpful contribution to synthesis of Fe-based materials.

Conflict of interest

The authors declare no conflict of interest.

Keywords: coordination polymers · dye-sensitized solar cells · hollow nanoparticles · iron pyrite · metal-organic frameworks · platinum-free

[1] C. Kantar, C. Ari, S. Keskin, *Water Res.* **2015**, *76*, 66–75.
[2] L. H. Kong, X. Y. Hu, M. C. He, *Environ. Sci. Technol.* **2015**, *49*, 3499–3505.
[3] L. Labiadh, M. A. Oturan, M. Panizza, N. Ben Hamadi, S. Ammar, *J. Hazard. Mater.* **2015**, *297*, 34–41.
[4] L. S. Li, M. Caban-Acevedo, S. N. Girard, S. Jin, *Nanoscale* **2014**, *6*, 2112–2118.
[5] Y. Bi, Y. B. Yuan, C. L. Exstrom, S. A. Darveau, J. S. Huang, *Nano Lett.* **2011**, *11*, 4953–4957.
[6] M. Cabán-Acevedo, M. S. Faber, Y. Z. Tan, R. J. Hamers, S. Jin, *Nano Lett.* **2012**, *12*, 1977–1982.
[7] M. Cabán-Acevedo, D. Liang, K. S. Chew, J. P. DeGrave, N. S. Kaiser, S. Jin, *ACS Nano* **2013**, *7*, 1731–1739.
[8] H. A. Macpherson, C. R. Stoldt, *ACS Nano* **2012**, *6*, 8940–8949.
[9] J. Puthussery, S. Seefeld, N. Berry, M. Gibbs, M. Law, *J. Am. Chem. Soc.* **2011**, *133*, 716–719.
[10] S. Shukla, N. H. Loc, P. P. Boix, T. M. Koh, R. R. Prabhakar, H. K. Mulmudi, J. Zhang, S. Chen, C. F. Ng, C. H. A. Huan, N. Mathews, T. Sritharan, Q. H. Xiong, *ACS Nano* **2014**, *8*, 10597–10605.
[11] Y. C. Wang, D. Y. Wang, Y. T. Jiang, H. A. Chen, C. C. Chen, K. C. Ho, H. L. Chou, C. W. Chen, *Angew. Chem. Int. Ed.* **2013**, *52*, 6694–6698; *Angew. Chem.* **2013**, *125*, 6826–6830.
[12] M. D. Wang, C. C. Xing, K. Cao, L. Zhang, J. B. Liu, L. Meng, *J. Mater. Chem. A* **2014**, *2*, 9496–9505.
[13] Z. H. Wei, Y. C. Qiu, H. N. Chen, K. Y. Yan, Z. L. Zhu, Q. Kuang, S. H. Yang, *J. Mater. Chem. A* **2014**, *2*, 5508–5515.
[14] J. Xu, H. T. Xue, X. Yang, H. X. Wei, W. Y. Li, Z. P. Li, W. J. Zhang, C. S. Lee, *Small* **2014**, *10*, 4754–4759.
[15] H. Y. Xian, J. X. Zhu, X. L. Liang, H. P. He, *RSC Adv.* **2016**, *6*, 31988–31999.
[16] D. W. Wang, Q. H. Wang, T. M. Wang, *CrystEngComm* **2010**, *12*, 3797–3805.
[17] B. B. Yu, X. Zhang, Y. Jiang, J. Liu, L. Gu, J. S. Hu, L. J. Wan, *J. Am. Chem. Soc.* **2015**, *137*, 2211–2214.
[18] M. G. Gong, A. Kirkeminde, S. Q. Ren, *Sci. Rep.* **2013**, *3*, 2092.

© 2017 Wiley-VCH Verlag GmbH & Co. KGaA, Weinheim

[19] Y. X. Bai, J. Yeom, M. Yang, S. H. Cha, K. Sun, N. A. Kotov, *J. Phys. Chem. C* **2013**, *117*, 2567 – 2573.
[20] R. Morrish, R. Silverstein, C. A. Wolden, *J. Am. Chem. Soc.* **2012**, *134*, 17854 – 17857.
[21] J. Wu, L. H. Liu, S. T. Liu, P. Yu, Z. R. Zheng, M. Shafa, Z. H. Zhou, H. D. Li, H. N. Ji, Z. M. M. Wang, *Nano Lett.* **2014**, *14*, 6002 – 6009.
[22] G. Smestad, A. Ennaoui, S. Fiechter, H. Tributsch, W. K. Hofmann, M. Birkholz, W. Kautek, *Sol. Energy Mater.* **1990**, *20*, 149 – 165.
[23] M. Wen, K. Mori, T. Kamegawa, H. Yamashita, *Chem. Commun.* **2014**, *50*, 11645 – 11648.
[24] M. Wen, K. Mori, Y. Kuwahara, H. Yamashita, *ACS Energy Lett.* **2017**, *2*, 1 – 7.
[25] M. Hu, S. Furukawa, R. Ohtani, H. Sukegawa, Y. Nemoto, J. Reboul, S. Kitagawa, Y. Yamauchi, *Angew. Chem. Int. Ed.* **2012**, *51*, 984 – 988; *Angew. Chem.* **2012**, *124*, 1008 – 1012.
[26] M. Hu, A. A. Belik, M. Imura, K. Mibu, Y. Tsujimoto, Y. Yamauchi, *Chem. Mater.* **2012**, *24*, 2698 – 2707.
[27] J. Wang, Q. Tang, B. He, P. Yang, *J. Power Sources* **2016**, *328*, 185 – 194.
[28] H. Zheng, C. Y. Neo, J. Ouyang, *ACS Appl. Mater. Interfaces* **2013**, *5*, 6657 – 6664.
[29] R. Jia, J. Chen, J. Zhao, J. Zheng, C. Song, L. Li, Z. Zhu, *J. Mater. Chem.* **2010**, *20*, 10829 – 10834.
[30] Q. Li, J. Wu, Q. Tang, Z. Lan, P. Li, J. Lin, L. Fan, *Electrochem. Commun.* **2008**, *10*, 1299 – 1302.
[31] S. Thomas, T. G. Deepak, G. S. Anjusree, T. A. Arun, S. V. Nair, A. S. Nair, *J. Mater. Chem. A* **2014**, *2*, 4474 – 4490.

Manuscript received: June 11, 2017
Accepted manuscript online: July 1, 2017
Version of record online: ■■ ▮▮, 0000

© 2017 Wiley-VCH Verlag GmbH & Co. KGaA, Weinheim

COMMUNICATION

Nanoparticles

J. E. Chen, M.-S. Fan, Y.-L. Chen, Y.-H. Deng, J. H. Kim, H. R. Alamri, Z. A. Alothman, Y. Yamauchi, K.-C. Ho, K. C.-W. Wu**

■■ – ■■

VIP **Prussian Blue-Derived Synthesis of Hollow Porous Iron Pyrite Nanoparticles as Platinum-Free Counter Electrodes for Highly Efficient Dye-Sensitized Solar Cells**

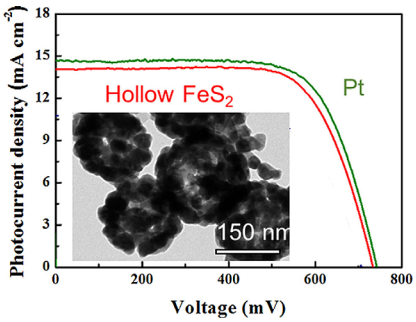

Caught the sun: Hollow porous iron pyrite nanoparticles were synthesized by a direct sulfurization of iron oxide derived from Prussian blue. The high efficiency of the hollow porous iron pyrite nanoparticles, as effective dye-sensitized solar cell counter electrodes, was demonstrated with an efficiency of 7.31 %.

© 2017 Wiley-VCH Verlag GmbH & Co. KGaA, Weinheim